MCB
Journals.ASM.org

Expression Profiling during Mammary Epithelial Cell Three-Dimensional Morphogenesis Identifies PTPRO as a Novel Regulator of Morphogenesis and ErbB2-Mediated Transformation

Min Yu,[a,b] Guang Lin,[a,b] Niloofar Arshadi,[d] Irina Kalatskaya,[d] Bin Xue,[a,b] Syed Haider,[d] Francis Nguyen,[d] Paul C. Boutros,[d] Ari Elson,[e] Lakshmi B. Muthuswamy,[d] Nicholas K. Tonks,[a,b] and Senthil K. Muthuswamy[a,b,c]

Cold Spring Harbor Laboratory, Cold Spring Harbor, New York, USA[a]; Graduate Programs in Genetics and Molecular and Cellular Biology, Stony Brook University, Stony Brook, New York, USA[b]; Ontario Cancer Institute, Campbell Family Institute for Breast Cancer Research, Department of Medical Biophysics, University of Toronto, Toronto, Canada[c]; Informatics and Biocomputing Platform, Ontario Institute for Cancer Research, Toronto, Canada[d]; and Department of Molecular Genetics, The Weizmann Institute of Science, Rehovot, Israel[e]

Identification of genes that are upregulated during mammary epithelial cell morphogenesis may reveal novel regulators of tumorigenesis. We have demonstrated that gene expression programs in mammary epithelial cells grown in monolayer cultures differ significantly from those in three-dimensional (3D) cultures. We identify a protein tyrosine phosphate, PTPRO, that was upregulated in mature MCF-10A mammary epithelial 3D structures but had low to undetectable levels in monolayer cultures. Downregulation of PTPRO by RNA interference inhibited proliferation arrest during morphogenesis. Low levels of PTPRO expression correlated with reduced survival for breast cancer patients, suggesting a tumor suppressor function. Furthermore, we showed that the receptor tyrosine kinase ErbB2/HER2 is a direct substrate of PTPRO and that loss of PTPRO increased ErbB2-induced cell proliferation and transformation, together with tyrosine phosphorylation of ErbB2. Moreover, in patients with ErbB2-positive breast tumors, low PTPRO expression correlated with poor clinical prognosis compared to ErbB2-positive patients with high levels of PTPRO. Thus, PTPRO is a novel regulator of ErbB2 signaling, a potential tumor suppressor, and a novel prognostic marker for patients with ErbB2-positive breast cancers. We have identified the protein tyrosine phosphatase PTPRO as a regulator of three-dimensional epithelial morphogenesis of mammary epithelial cells and as a regulator of ErbB2-mediated transformation. In addition, we demonstrated that ErbB2 is a direct substrate of PTPRO and that decreased expression of PTPRO predicts poor prognosis for ErbB2-positive breast cancer patients. Thus, our results identify PTPRO as a novel regulator of mammary epithelial transformation, a potential tumor suppressor, and a predictive biomarker for breast cancer.

Loss of proliferation control is a property of cancer cells. Understanding the mechanisms by which epithelial cells control proliferation will identify novel ways to understand and treat cancer. Resting mammary epithelial cells typically remain in a low proliferation state *in vivo* (5). When nontransformed mammary epithelial cells, such as MCF-10A, are cultured on Matrigel, a reconstituted basement membrane, they form three-dimensional (3D) acinar structures (30). The morphogenesis of these structures recapitulates the pattern of growth and differentiation seen in the terminal duct lobular units (TDLUs) in the mammary gland *in vivo* (7, 9). Each single cell plated in this 3D culture system proliferates to form a sphere of cells; the cells in the interior of the spheres, which lack attachment to the basement membrane, are eliminated by both apoptotic and nonapoptotic cell death mechanisms (8). This development phase is followed by a phase of maturation that involves compaction of the structure and acquisition of a proliferation arrest. The resulting acinus-like structures have properties such as polarization, 3D organization, and proliferation control that are akin to those observed in human breast acini *in vivo*. However, they are not terminally differentiated, as demonstrated by their ability to proliferate and form new acini in a manner similar to that of the parental cells in the breast when acini are disrupted and plated onto new 3D cultures (30).

It is likely that MCF-10A cells use distinct mechanisms to achieve and maintain proliferation arrest in monolayer (2D) and in 3D culture. For example, we have previously demonstrated that overexpression of cyclin D1 or activation of ErbB2 regulates cell proliferation differently in 2D and 3D cultures (8, 30). Although MCF-10A cells expressing these oncogenes retain the ability to achieve proliferation arrest by contact inhibition when grown in monolayer cultures, they fail to undergo proliferation arrest in 3D culture, demonstrating that MCF-10A cells use different mechanisms to reach proliferation arrest during contact inhibition and 3D morphogenesis. To begin to obtain direct insights into the molecular mechanisms by which cells in 3D and 2D monolayer culture reach proliferation arrest, we have identified global gene expression signatures associated with proliferation arrest under both conditions. We report that cell culture conditions exert a major influence on gene expression, and we have identified genes that are specific to the proliferation-arrested state in either 2D monolayer cultures or 3D acini. By analyzing genes that were upregulated in proliferation-arrested 3D acini, we discovered a novel

Received 14 January 2012 Returned for modification 4 February 2012
Accepted 23 June 2012
Published ahead of print 30 July 2012
Address correspondence to Senthil K. Muthuswamy, S.muthuswamy@utoronto.ca.
Supplemental material for this article may be found at http://mcb.asm.org/.
Copyright © 2012, American Society for Microbiology. All Rights Reserved.
doi:10.1128/MCB.00068-12

role for the protein tyrosine phosphatase PTPRO during 3D morphogenesis.

Initially identified as GLEPP1, a renal glomerular podocyte protein, PTPRO is a transmembrane receptor-like PTP (39, 41). There are multiple variants of PTPRO, which arise from the use of distinct promoters and through alternative splicing, leading to a variable extracellular segment (25). PTPRO has been implicated in several biological processes, including neuronal outgrowth (3), axonal guidance (13, 35), and osteoclast function (14), with links established between PTPRO and particular signaling pathways, including regulation of SYK in B cell signaling (4, 18), c-Kit (38), WNT (19), and BCR-ABL (27). Here, we demonstrate that loss of PTPRO cooperates with ErbB2 to transform mammary epithelial acini and that decreased expression of PTPRO is a prognostic factor in breast cancer.

MATERIALS AND METHODS

Materials. MCF-10A cells were obtained from ATCC (Manassas, VA) and cultured in Dulbecco's modified Eagle medium (DMEM)–F-12 (Invitrogen) supplemented with 5% donor horse serum, 20 ng/ml epidermal growth factor (EGF), 10 μg/ml insulin, 100 ng/ml hydrocortisone, 100 ng/ml cholera toxin, 100 U/ml penicillin, and 100 μg/ml streptomycin. The dimerizing compound, AP1510, was obtained from ARIAD Pharmaceuticals. Growth factor-reduced Matrigel was purchased from BD Biosciences; the protein concentration of the lots used ranged from 9 to 11 mg/ml. Microarray chips (HG-U133A) were purchased from Affymetrix.

The following primers for quantitative real-time (RT)-PCR were purchased from Sigma: PTPRO, 5′-TTCAGAGGAAGAGCAGGACGAC and 3′-CATCCTGCATCTCGTCAGCATA; and GAPDH, 5′-AAATTCCATG GCACCGTCAA and 3′-TCTCGCTCCTGGAAGATGGT. Isoform-specific RT-PCR was performed using P1, 5′-TTCAGAGGAAGAGCAGGA CGAC-3′ and 5′-CATCCTGCATCTCGTCAGCATA-3′; P2, 5′-AAGTT GGCTCCAGTCAGAAAACC-3′ and 5′-TTGTAGGCAGTGGCAGGAA GAAGG-3′; P3, 5′-TGAGACAGAGAAGTCAACATCAGGC-3′ and 5′-G GAACCCATCAAAAGCAGTGG-3′; P4, 5′-GCACTCAGGTGAACTCA AGCAAAC-3′ and 5′-AGGTGGTCCAATCAAAGGGC-3′; P5, 5′-GCTG GATTGGACACTCCTAAAACC-3′ and 5′-AAGGGCTCACATAATGG GGG-3′; and P6, 5′-AAGACATTCAGACCCACAGAAAGG-3′ and 5′-C ACCACTGCTCTCACTATGCTCAG-3′.

The small hairpin RNAs (shRNAs) against human PTPRO were designed by using computer software (www.cshl.org/public/SCIENCE/hannon.html), and the targeting sequences that were used to silence gene expression were A, CTCACTCAGTGTAATGAGA; B, CACAGCAAATGCTGCAGAA; and C, GCCAAAGACTCTGACTATA. The vector MSCV-LTR-PURO-IRESGFP (MLP) was kindly provided by the Scott Lowe, Cold Spring Harbor Laboratories.

Anti-Ki67 antibody was from Calbiochem. Anti-cleaved caspase 3 was from Cell Signaling. Anti-phosphotyrosine 4G10 and PT66 were from Upstate Biotechnology and Sigma, respectively. Antihemagglutinin (anti-HA) was from Covance, and anti-His tag from Qiagen. Anti-mouse or anti-rabbit antibodies conjugated with Alexa Fluor dyes were from Molecular Probes. Goat $F(ab')_2$ anti-mouse IgG (H+L) was from Caltag Laboratories. Antifade agent Prolong was from Molecular Probes.

The rabbit polyclonal anti-PTPRO antibody was generated against the peptide DCTNPVQLDDFDSYIKDMAKDS, which is common to all known protein products of the PTPRO gene. The antibody is capable of recognizing endogenous PTPRO in tissues and exogenous PTPRO in transfected cells. A detailed description of this antibody will be published elsewhere.

Morphogenesis assay. The three-dimensional culture of MCF-10A cells on basement membrane was carried out as previously described (30). Briefly, four-well chamber RS glass slides (BD) were coated with 100 μl of Matrigel per well and left to solidify for 20 min at 37°C. Cells were trypsinized and resuspended in DMEM–F-12 supplemented with 20% donor horse serum. The cells were spun down and resuspended in assay medium (DMEM–F-12 supplemented with 2% donor horse serum, 10 μg/ml insulin, 100 ng/ml hydrocortisone, 100 ng/ml cholera toxin, 100 U/ml penicillin, and 100 μg/ml streptomycin) containing 2.5% Matrigel and 5 ng/ml EGF at a concentration of 5×10^4 per 4 ml. A 400-μl volume of cell suspension was added to each well, and assay medium containing 5 ng/ml EGF was replaced every 4 days. For the 2D culture used in the microarray study, MCF-10A cells were plated at a concentration of 0.75×10^5 per well on 6-well plates coated with a very thin layer of Matrigel (BD) in the same assay medium as mentioned above. For stimulation of ErbB2, EGF-containing assay medium with 1 mM AP1510 was replaced on day 4 (for 2D cultures) or 15 (for 3D cultures); cultures were refed every 2 days with the stimulation medium.

RNA extraction. Total RNA was isolated by phenol-chloroform extraction (TRIzol; Invitrogen) according to the manufacturer's protocols.

Array hybridization. RNA was quantified using Agilent 2100 Bioanalyzer before processing to prepare for array hybridization. RNA samples were prepared according to the Affymetrix GeneChip Analysis manual. Basically, a total of 5 μg RNA is first reverse transcribed using a T7-oligo(dT) promoter primer in the first-strand cDNA synthesis reaction. Following RNase H-mediated second-strand cDNA synthesis, the double-stranded cDNA was purified and served as a template in the subsequent *in vitro* transcription (IVT) reaction. The IVT reaction was carried out in the presence of T7 RNA polymerase and a biotinylated nucleotide analog/ribonucleotide mix for cRNA amplification and biotin labeling. The biotinylated cRNA targets were then cleaned up, fragmented, and hybridized to GeneChip expression arrays at 45°C for 16 h in a rotation oven. The hybridized chips were subjected to washes and staining in a Fluidics Station 450. Finally, the arrays were scanned by Affymetrix Genechip Scanner 3000 and processed automatically into digital CEL files.

Data processing. All the CEL files from different replicates and experimental conditions were used directly in the normalization step. Single values from each of the probe sets were calculated and normalized by means of the robust microarray analysis (RMA) (16) method using Bioconductor (http://www.bioconductor.org) in the R computing environment. Scatter plots of replicates were done in R.

For clustering, Affymetrix Microarray Suite 5.0 (MAS5) was used to generate the intensity file for each experiment, and hierarchical clustering was done using MEV4.0, developed by the J. Craig Venter institute (33). Data were filtered based on a good signal (software parameter "P" or detected signal above threshold) and retained if there was a good signal of the gene from at least two experiments of 2D and at least three experiments in 3D. Those that did not meet the criteria were removed from the cluster. The image was generated using the ratio of absolute intensity to the median of all the genes in all experiments.

For data normalization, we used the hgu133a.db package in R. We used the following methods in each step: RMA for background correction, quantile for normalization, pm only for PM correction, and median polish for summarization. Fold change is calculated by dividing the raw expression level of each gene in the first experiment by the expression level of the corresponding gene in the second experiment; and *P* values in fold change were calculated using the analysis of variance (ANOVA) test.

For pathway analysis, we used the Reactome/KEGG functional interaction (FI) network, cytoscape plug-in (42), to identify the significant pathways. The binomial test was used for functional enrichment analysis. The FDR (false discovery rate) was calculated based on 1,000 permutations on all genes in the FI network. Only pathways with *P* values of <0.05 and FDR of <0.1 were taken into consideration.

For expression analyses in breast cancer patients, we combined six breast cancer data sets containing in total 16,785 genes from 922 samples (238 of these patients survived and 684 did not). Details of subjects are given elsewhere for the six data sets, which respectively comprised 158 samples (2), 198 samples (10), 77 samples (21), 236 samples (23), 159 samples (31), and 94 samples (37). We ranked genes with *P* values of ≤ 0.05 based on their fold change in 3D morphogenesis and selected the

top 20 genes to validate in the breast cancer patient tumor expression data. In our box plots, we compared the gene expression values of subjects who survived less than 5 years (103 subjects) with those of subjects who survived more than 10 years (318 subjects) and report the two-sided *t* test *P* value.

Quantitative real-time PCR. Total RNA (2 μg) was reverse transcribed into cDNA using the TaqMan probe kit (Applied Biosystems) by following the manufacturer's instructions. Primers for selected genes were designed via the Primer Express software (version 1.5a; PE Applied Biosystems). To avoid genomic DNA contamination, primers were designed to overlap the exon-exon boundary. Primers were also subjected to BLAST analysis against the RefSeq known transcripts for uniqueness. Quantitative RT-PCR included the following: diluted cDNA sample, 0.5 μmol/liter primers, nucleotides, *Taq* DNA polymerase, and the buffer included in the SYBR green I Mastermix (Applied Biosystems). Using the ABI Prism 7700 sequence detection system (Applied Biosystems), PCR cycling conditions were as follows: 50°C for 2 min, 95°C for 10 min, 40 cycles at 94°C for 15 s, and 60°C for 1 min. Sequence Detector Software (version 1.9.1; Applied Biosystems) was used to extract the PCR data, which were then exported to Excel (Microsoft, Redmond, WA) for further analysis. Expressions of target genes were measured in triplicate and normalized to GAPDH expression levels.

Generation of cell lines stably expressing the shRNA construct. To generate the retrovirus, 10 μg plasmid DNA was transfected into the vesicular stomatitis virus-glycoprotein G (VSV-GPG) retrovirus packaging cell line by standard calcium phosphate methods. Media containing viruses were collected at days 4, 5, and 6 after transfection and passed through a 0.45-μm filter. Medium was then overlaid on MCF-10A cells with 8 μg/ml Polybrene added. Forty-eight hours later, pools were generated by selection in 2.0 μg/ml puromycin for 2 days. Stable suppression of proteins was confirmed by immunoblotting.

Immunoblotting. For the cells in acinar structures on Matrigel (3D), structures were washed with room temperature phosphate-buffered saline (PBS) and isolated from Matrigel using a nonenzymatic solution, Cell Recovery Solution from BD Biosciences, on ice for 30 min. Cells were collected by centrifugation at 4°C at 6,000 rpm for 3 min and washed twice with chilled PBS. Cells from 3D acinar structure or plastic dishes (2D) were lysed with radioimmunoprecipitation assay (RIPA) buffer on ice for 30 min. The lysate was centrifuged at 4°C at 13,000 rpm for 15 min. The supernatant was added to SDS sample buffer and boiled at 100°C for 5 min. Equal amounts of protein were separated by SDS-PAGE, transferred to polyvinylidene difluoride (PVDF) membrane, and probed with appropriate primary antibodies and then horseradish peroxidase (HRP)-conjugated secondary antibodies. Immunoreactive bands were visualized with the enhanced chemiluminescence (ECL) system. Protein levels were quantified using Image J (NIH) software.

Acinus size quantitation. Phase images of 3D acinus structures were taken at different days with a 10× objective. The structure area was measured using AxioVision 4.4 software (Zeiss). At least 600 images from three different experiments were studied for each experimental condition, and areas were subjected to the Wilcoxon signed rank test for statistical significance of differences between conditions. The Wilcoxon signed rank test and the box plot were done via the statistical computation program R.

3D immunofluorescence and microscopy. The immunofluorescence analysis was conducted as described previously (9). Briefly, 3D acinar structures were washed with PBS, fixed with 2% paraformaldehyde for 30 min at room temperature, washed three times with PBS-glycine, permeabilized with 0.5% Triton X-100 for 10 min, and washed three times with washing buffer. The structures were then blocked with 10% goat serum in washing buffer for 1 h, blocked with a secondary block of goat anti-mouse $F(ab')_2$ fragment diluted 1:100 in primary block for 30 min, and then incubated with proper primary antibodies (1:100 dilutions) overnight, washed three times with washing buffer, blocked with secondary antibodies conjugated with Alexa Fluor dyes for 1 h, washed three times, and incubated with 4′,6-diamidino-2-phenylindole (DAPI) for 10 min. Slides were mounted with the antifade agent Prolong. Microscopy was performed on Zeiss Axiovert 200 M using the AxioVision 4.4 and ApoTome imaging system.

Construction, expression, and purification of recombinant His-tagged PTP domain of PTPRO. The wild-type full-length PTPRO expression construct was purchased from Origene. To generate the substrate-trapping mutant form of PTPRO, point mutation D1102A was introduced into the PTP domain of PTPRO using the QuikChange site-directed mutagenesis kit (Stratagene). After mutagenesis, the PTP domain of the wild-type construct and the substrate-trapping, D1102A PTPRO (amino acids T915 to S1216) mutant was subcloned to the bacterial expression vector pET28a. The recombinant protein of the wild-type construct and the substrate-trapping, the D1102A PTPRO mutant PTP domain was generated according to the method described previously by Lin et al. (20).

Substrate-trapping pulldown assay. For the substrate-trapping pulldown, 1 μg of the purified recombinant PTPRO (from the wild type or from the substrate-trapping, D1102A mutant) was prebound to the Ni-nitrilotriacetic acid (Ni-NTA) beads. After washes, prebound Ni-NTA beads were used to pull down interacting proteins from 100 μg of pervanadate-treated MCF10A/ErbB2 lysate at 4°C overnight. Following pulldown, the Ni-NTA beads were washed by lysis buffer and then were eluted by sample buffer. The pulldown of the chimeric ErbB2 was detected by anti-HA blotting.

RESULTS

Gene expression profiles of morphogenesis in 3D and 2D cultures. To compare the genes that are associated with acquisition of proliferation arrest in 2D and 3D cultures, we compared gene expression changes between day 2 (actively dividing) and day 5 (contact-inhibited) 2D monolayers and day 8 (growing) and day 16 (proliferation-arrested, mature) 3D acini (Fig. 1A). To control for variations between biological samples, we repeated the experiment five times. The integrity and quality of RNA were assessed on denaturing agarose gels and by analyzing the RNA in an Agilent 2100 BioAnalyzer before processing for microarray analysis. We used Affymetrix HG-U133A chips, which contain ProbeSets for 18,400 transcripts and variants in the human genome, and data from all the conditions were normalized using robust multiarray analysis (RMA) (16). The correlation coefficients of the hybridization intensity calculated between each pair of replicates under a particular condition were all above 0.96, indicating reproducibility.

To determine the relationship between gene expression patterns observed under the different culture conditions, we performed unsupervised two-way hierarchical clustering for changes associated with all genes reproducibly altered in expression in more than two biological replicates and related them to the experimental conditions. Interestingly, samples from 3D acini and from 2D monolayers segregated independently of each other (Fig. 1B), demonstrating that the overall gene expression pattern observed in cells grown in 3D resembles more closely that of other samples from 3D than it does the gene expression patterns observed in cells grown as 2D monolayers, irrespective of the proliferation status.

To understand the influence of culture conditions on changes in gene expression, we identified genes that vary more than 1.5-fold with reproducible changes among the biological replicates ($P < 0.05$) for different biological states. In cells undergoing proliferation arrest in monolayer cultures (day 2 versus day 5), 323 genes differ significantly in expression (Fig. 1C; see Table S1 in the supplemental material) and belong to pathways related to cell cycle, integrin, and p53 signaling pathways (Table 1). In contrast, in

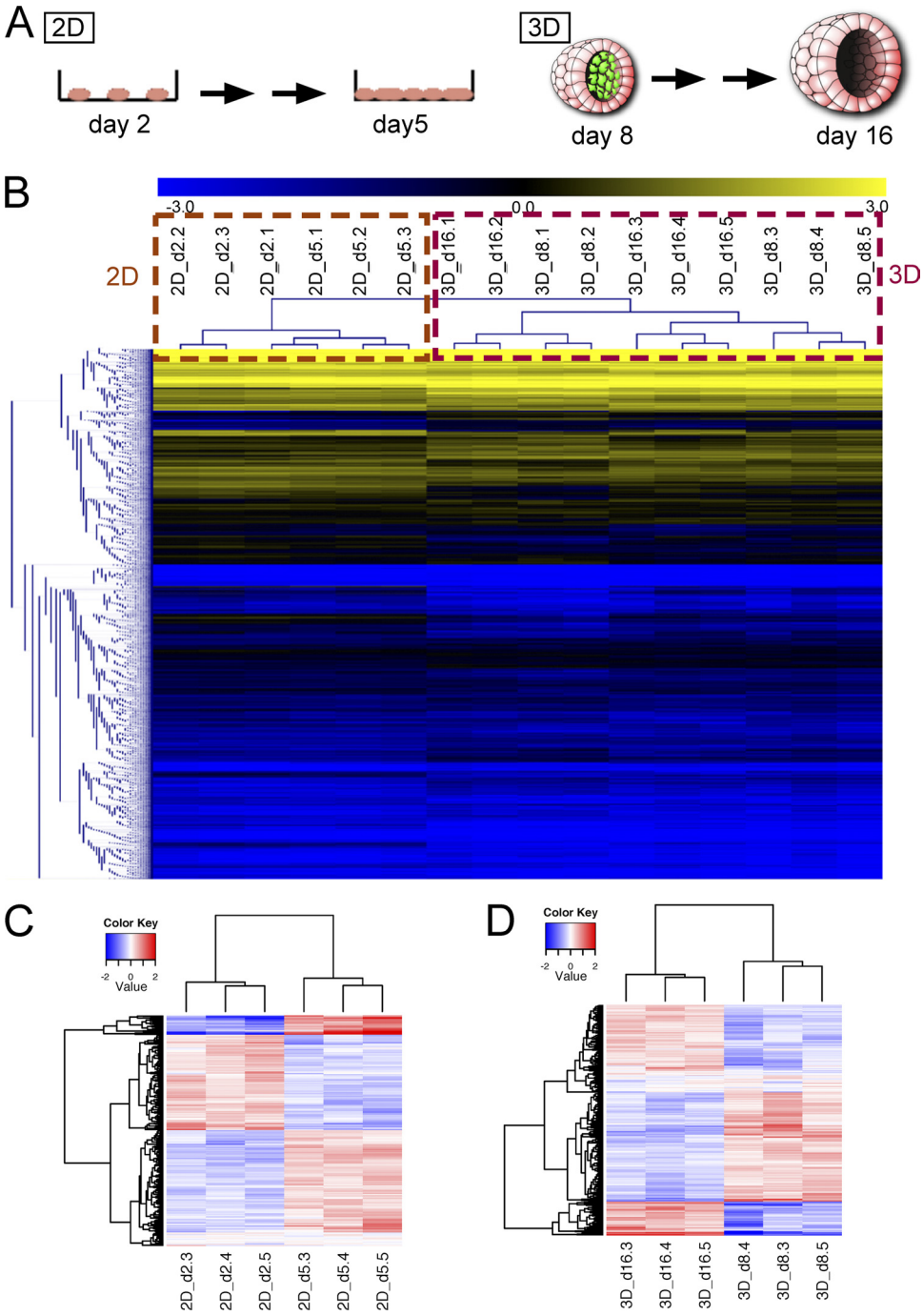

FIG 1 Gene expression analysis of proliferation arrest in 2D and 3D cultures. (A) Illustration of microarray designs for 2D and 3D cultures. MCF-10A cells were plated in 2D and in 3D cultures. Total mRNAs were extracted from cells at day 2 and day 5 in 2D, as well as at day 8 and day 16 in 3D, and were hybridized onto Affymetrix HGU-133A arrays. (B) Two-way hierarchical clustering of gene expressions from all the conditions. Genes are in rows, and experiments are in columns. Data plotted were the ratios of intensity value of each gene at each experiment over the mean value of all data points. Yellow represents positive ratios, and blue represents negative ratios. (C) Hierarchical clustering of differentially expressed genes in 2D at day 2 and day 5. (D) Hierarchical clustering of differentially expressed genes in 3D at day 8 and day 16.

cells undergoing proliferation arrest in 3D culture (day 8 versus day 16), 344 genes differ significantly in expression (Fig. 1D; see Table S2 in the supplemental material) and represent ceramide, tumor necrosis receptor, spingosine-1-phosphate, and *Escherichia coli* infection signaling pathways (Table 2). These observations demonstrate that mammary epithelial cells use different mechanisms to undergo proliferation arrest in monolayer and in 3D cultures.

We compared proliferating or proliferation-arrested cells in 2D and 3D. More than 2,000 genes were differentially expressed in

TABLE 1 Pathways represented by genes that are differentially regulated during proliferation arrest in monolayer cultures

Pathway	No. of proteins		*P* value	FDR	Gene IDs
	In pathway	From study			
p53 signaling pathway	12	4	2.062e−04	5.900e−02	*CCND1*, *CCNE1*, *CDKN1A*, *GADD45A*
FOXM1 transcription factor network	38	6	3.115e−04	4.200e−02	*AURKB*, *CCND1*, *CCNE1*, *CENPA*, *ETV5*, *FOXM1*
p53 signaling pathway	54	7	3.236e−04	2.867e−02	*CCNG2*, *DDB2*, *GADD45A*, *GTSE1*, *PERP*, *SERPINE1*, *THBS1*
Cell cycle	112	10	3.543e−04	2.300e−02	*BUB1B*, *CCNA1*, *CCND1*, *CCNE1*, *CDC25A*, *CDC6*, *CDKN1A*, *CDKN1C*, *DBF4*, *GADD45A*
G_1/S transition	98	9	5.743e−04	3.160e−02	*CCNA1*, *CCNE1*, *CDC25A*, *CDC6*, *CDKN1A*, *DBF4*, *FBXO5*, *MCM10*, *PRIM1*
Aurora A signaling	62	7	7.291e−04	3.350e−02	*AURKA*, *AURKB*, *CENPA*, *GADD45A*, *MALT1*, *NFKBIA*, *TNFAIP3*
Telomere maintenance	30	5	7.836e−04	3.114e−02	*FEN1*, *POLD4*, *PRIM1*, *RFC3*, *TINF2*
Cyclins and cell cycle regulation	19	4	1.142e−03	4.138e−02	*CCNA1*, *CCND1*, *CCNE1*, *CDKN1A*
Cell cycle: G_1/S checkpoint	22	4	1.944e−03	6.022e−02	*CCNA1*, *CCND1*, *CCNE1*, *CDKN1A*
DNA replication	95	8	1.992e−03	5.560e−02	*CDC6*, *CDKN1A*, *DBF4*, *FEN1*, *MCM10*, *POLD4*, *PRIM1*, *RFC3*
S phase	97	8	2.263e−03	5.645e−02	*CCND1*, *CDC25A*, *CDC6*, *CDKN1A*, *FEN1*, *POLD4*, *PRIM1*, *RFC3*
Integrin signaling	39	5	2.460e−03	5.575e−02	*CTGF*, *CYR61*, *FN1*, *PLAU*, *PLAUR*
p53 pathway	58	6	2.690e−03	5.746e−02	*CCNE1*, *DDB2*, *GADD45A*, *GTSE1*, *PERP*, *THBS1*

proliferating cells grown in monolayer cultures compared to proliferating cells grown in 3D cultures (see Fig. S1A and Table S3 in the supplemental material). More than 1,700 genes were differentially expressed in proliferation-arrested cells in monolayer cultures compared to those in 3D cultures (see Fig. S1B and Table S4 in the supplemental material). These genes represent a large number of signaling pathways (see Tables S3 and S4 in the supplemental material), demonstrating that cells cultured in 2D and 3D display significant differences in gene expression programs involving multiple signaling pathways, irrespective of their proliferation status.

Regulation of proliferation arrest during 3D morphogenesis. We reasoned that genes that are upregulated during proliferation arrest in acini may represent a novel class of candidate tumor suppressors because they are likely to promote and/or maintain proliferation arrest during normal morphogenesis. To identify the clinical significance of the genes upregulated in 3D acini, we analyzed the relationship between changes in gene expression level and survival of breast cancer patients. We used a data set representing 922 primary breast tumors with associated patient survival data more than 10 years postdiagnosis (6) developed by compiling data from six studies, each monitoring gene expression changes of a total of 16,785 genes. The expression level of each gene upregulated in 3D acini of patients who died within 5 years ($n = 103$) was compared to that of patients who survived for more than 10 years ($n = 318$) after diagnosis (Fig. 2). Among the top 20 genes analyzed, those encoding PTPRO (a protein tyrosine phosphatase) (Fig. 2), ZMYND6 (unknown function) (see Fig. S2D in the supplemental material), and SRSF7 (splicing factor) (see Fig. S2H) showed a correlation between loss of expression and reduced patient survival; the remaining 17 genes did not show either a significant correlation with patient survival or a relationship between higher levels of expression and decreased patient survival ($P < 0.05$) (Fig. 2; see Fig. S2 in the supplemental material). We selected PTPRO for further functional analysis to explore its potential tumor suppressor role and to understand the relationship between its expression and transformation of mammary epithelial cells.

Suppression of PTPRO increased acinar size. To validate the increase in PTPRO expression detected in microarrays of proliferation-arrested 3D acini, we analyzed both RNA and protein levels of this phosphatase. PTPRO mRNA levels analyzed for changes in expression of two long-form transcripts and two short-form transcripts (see Fig. S4 in the supplemental material) or using primers that recognize all splice variants (Fig. 3A) showed a 4-fold upregulation in proliferation-arrested acini compared to the actively growing structures. Although the protein levels were unde-

TABLE 2 Pathways represented by genes that are altered during proliferation arrest in 3D cultures

Pathway	No. of proteins		*P* value	FDR	Gene IDs
	In pathway	From study			
Ceramide signaling	47	7	1.338e−04	3.600e−02	*AIFM1*, *BID*, *BIRC3*, *MYC*, *NFKBIA*, *PDGFA*, *PRKRA*
Pathogenic *E. coli* infection	26	5	3.989e−04	4.850e−02	*ACTB*, *TUBA1B*, *TUBB*, *TUBB2C*, *TUBB3*
Tumor necrosis factor receptor signaling	272	16	6.667e−04	5.567e−02	*AIFM1*, *BCL3*, *BID*, *BIRC3*, *CYLD*, *FOS*, *LYN*, *MYC*, *NFKBIA*, *PDGFA*, *PPARG*, *PRKCH*, *PRKRA*, *PTPRK*, *SLC3A2*, *SQSTM1*
Sphingosine 1-phosphate	130	10	1.041e−03	7.250e−02	*AIFM1*, *BID*, *BIRC3*, *FOS*, *GRB10*, *LYN*, *MYC*, *NFKBIA*, *PDGFA*, *PRKRA*

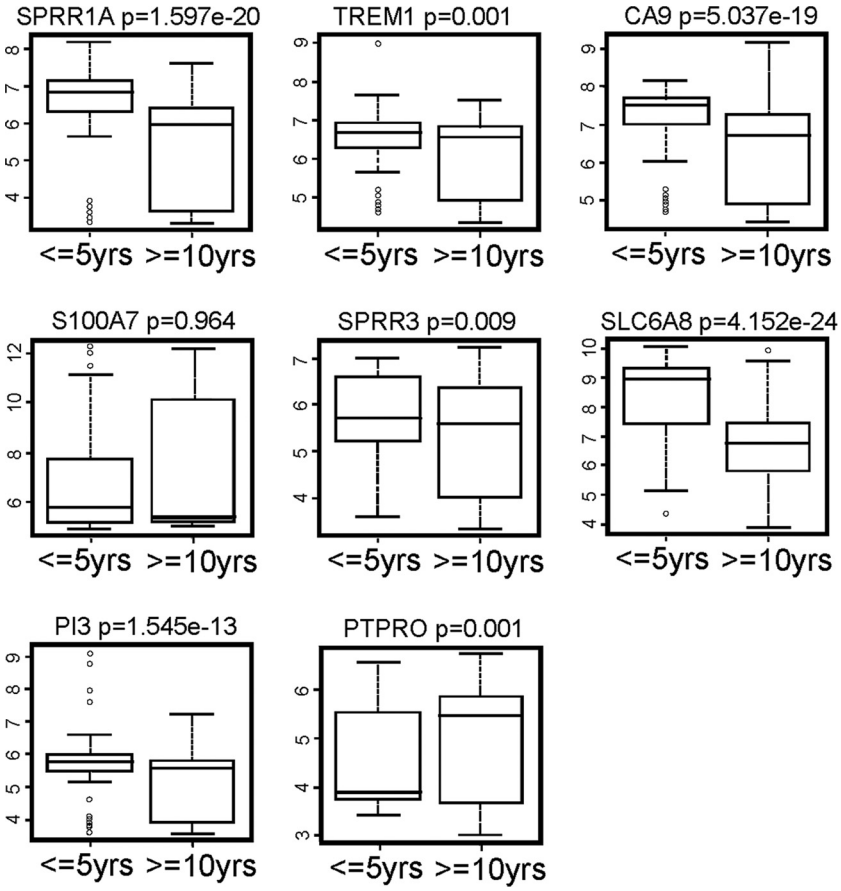

FIG 2 Box plots of gene expression levels in breast cancer patients for the top eight upregulated genes during proliferation arrest identified in 3D cultures. *P* values are shown above the plots.

tectable in lysates from growing structures, PTPRO was upregulated in day 16 cell lysates (Fig. 3B, compare shLuc lanes), consistent with the microarray analysis.

To investigate if the changes in PTPRO expression play a functional role during morphogenesis, we suppressed PTPRO expression using RNA interference (RNAi) (see Fig. S5A in the supplemental material). Stable cell populations expressing specific short hairpin RNAs targeting PTPRO were plated in 3D matrix. Two (A and C) of the three short hairpins showed effective suppression of PTPRO and increased acinar size ($P < 0.001$) (see Fig. S4 in the supplemental material). We chose short hairpin C for further studies. RNAi-mediated knockdown of PTPRO protein level was confirmed using cell lysates from proliferation-arrested 3D structure (Fig. 3B). PTPRO-suppressed cells displayed increased acinar size at both day 8 and day 16 compared to control cells (Fig. 3C, D, and E) ($P < 0.0001$). These observations revealed a functional role for PTPRO in determining acinar size during 3D morphogenesis.

PTPRO regulated proliferation arrest, but not cell death, during morphogenesis. The size of MCF-10A cell acini is determined by a balance between cell proliferation and death (7). To understand the process that leads to an increase in acinar size, we investigated changes in cell proliferation and apoptosis during morphogenesis, using Ki67 as a proliferation marker and cleaved caspase-3 as a marker for apoptosis. Acini derived from PTPRO-suppressed cells displayed a consistent increase in the number of Ki67-positive cells (Fig. 4A and C); in particular, acini derived from PTPRO-suppressed cells failed to undergo proliferation arrest by day 14 compared to acini derived from control cells, which arrested at day 10. However, there was no difference in the cleavage of caspase 3, suggesting that suppression of PTPRO did not affect the rates of cell death (Fig. 4B and D). Together, these results suggest that the increase in size of acini that accompanied suppression of PTPRO was due to impaired proliferation arrest.

Suppression of PTPRO cooperated with ErbB2 in promoting proliferation. Although downregulation of PTPRO resulted in a hyperproliferative phenotype, it did not transform the 3D acini. We reasoned that whereas loss of PTPRO may not be a potent transforming event on its own, it may augment the transforming ability of oncogenes such as HER2/ErbB2. Previously, we have used a chimeric ErbB2 receptor and a small-molecule dimerizing ligand (see Fig. S5 in the supplemental material for a description of the method) to show that dimerization and activation of ErbB2 in MCF-10A 3D acini disrupt proliferation arrest and induce formation of multiacinar structures (30). Here, we show that suppression of PTPRO cooperated with activation of ErbB2 to induce multiacinar structure formation (Fig. 5A and B), with a significant increase in acinar size in shPTPRO cells (median, 1,996 μm^2) compared to shLuc cells (median, 1,732 μm^2) after ErbB2 activation ($P < 0.0001$). Loss of PTPRO significantly enhanced ErbB2-induced proliferation, as monitored by analysis of proliferation

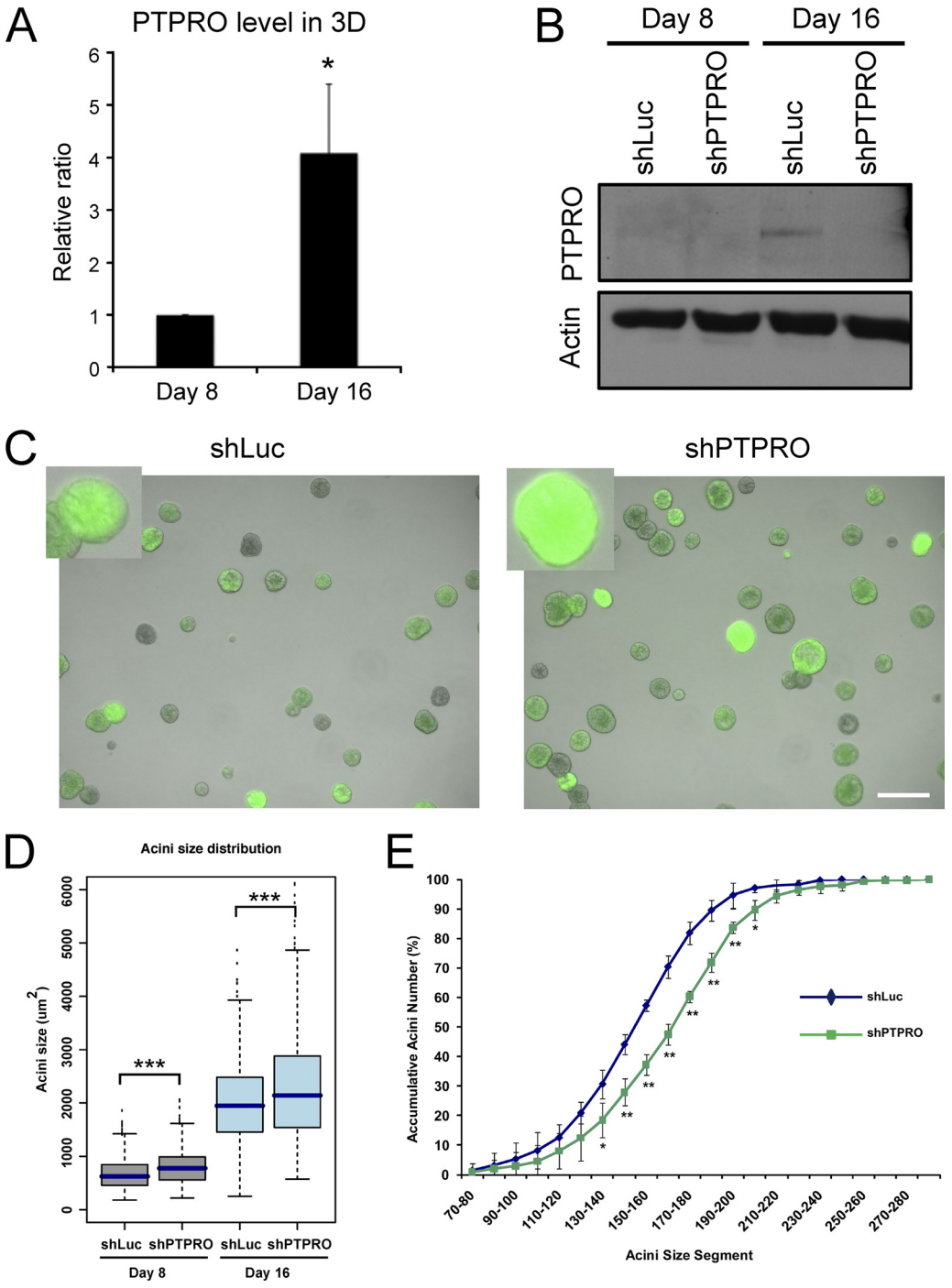

FIG 3 Suppression of PTPRO increased acinar size. (A) Quantitative RT-PCR validation of PTPRO expression changes during 3D morphogenesis. Results were normalized to endogenous GAPDH control, and the relative ratios of day 16 to day 8 were plotted ($n = 3$; *, $P < 0.05$; data are means ± standard deviations). (B) Analysis of protein level of PTPRO in 3D morphogenesis in shLuc and shPTPRO cells by Western blotting. (C) Phase images of acinar structures of PTPRO-suppressed cells (shPTPRO) and control cells (shLuc) in 3D at day 12 (scale bar = 100 μm). Expression of green fluorescent protein identifies acini derived from cells expressing the PTPRO shRNA. (D) Distribution of acinar sizes at day 8 and day 16 structures plotted in box plots. Each condition represented at least 600 acini from three independent experiments (***, $P < 0.001$). (E) Distribution of acinar sizes at day 16 plotted in segment accumulative plot. Acinar sizes were grouped into indicated segments. The number of acini that fitted to each size segment was determined and plotted as accumulative number in percentages ($n = 3$; *, $P < 0.05$; **, $P < 0.01$).

marker Ki67, consistent with the observations in parental MCF-10A cells (Fig. 5C). The percentage of acini with multiple (>3) Ki67-positive cells was significantly higher following suppression of PTPRO in ErbB2-expressing MCF-10A (11) than in the control cells (Fig. 5D). These results indicate that suppression of PTPRO cooperated with activation of ErbB2 to induce cell proliferation.

ErbB2 was a direct substrate of PTPRO. To understand the mechanism by which loss of PTPRO cooperated with activation of

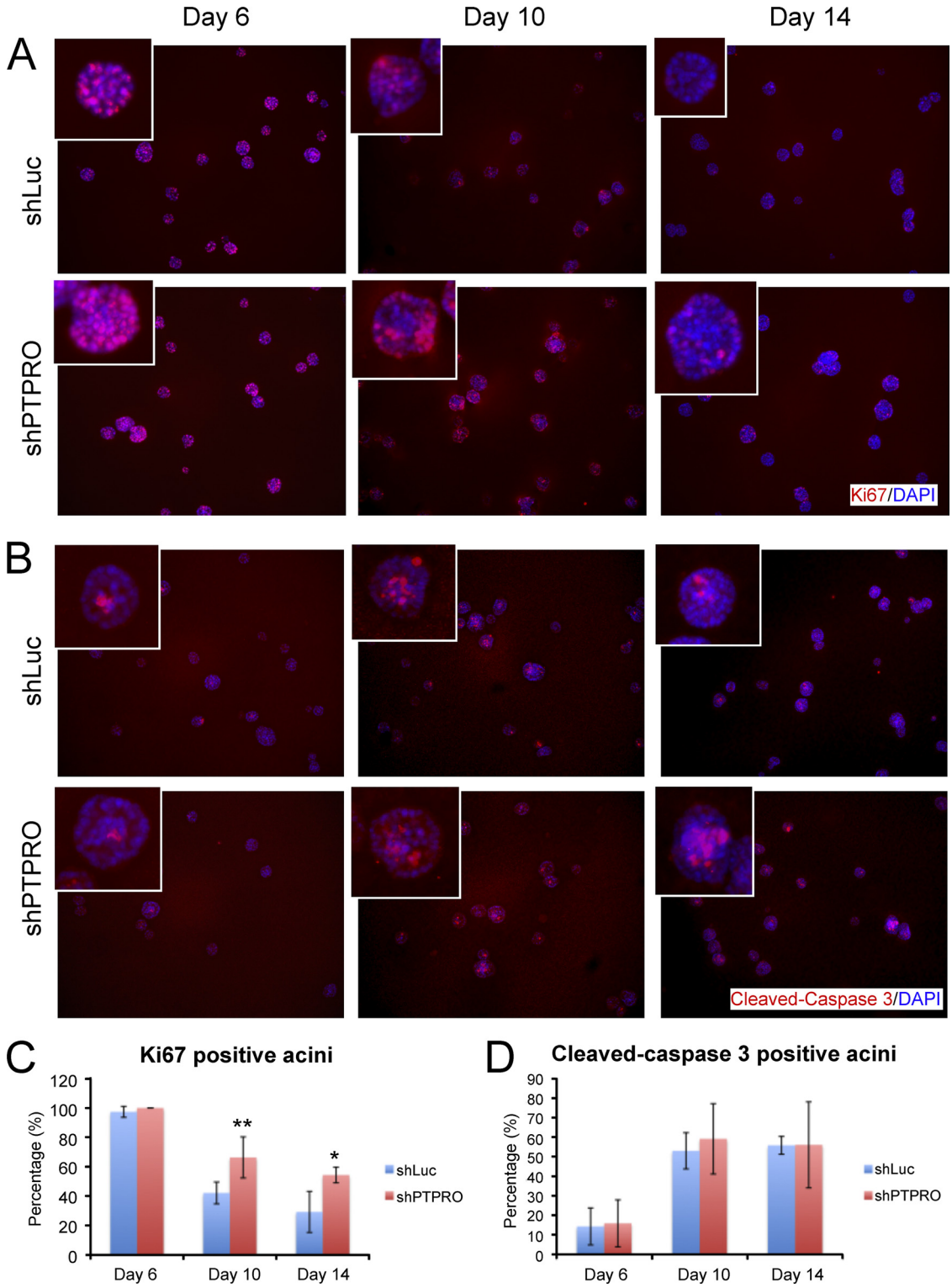

FIG 4 PTPRO regulated proliferation arrest but not cell death during morphogenesis. PTPRO-suppressed cells (shPTPRO) and control cells with shRNA for luciferase (shLuc) were grown in 3D cultures, and immunofluorescence assays were performed on day 6, day 10, and day 14 for proliferation marker and apoptosis marker. Scale bar = 100 μm. (A) Cells were probed with anti-Ki67 (red) antibody for active proliferation. Nuclei were stained by DAPI (blue). (B) Cells were probed with apoptotic marker cleaved-caspase 3 antibody (red). (C) Quantification of percentage of Ki67-positive acini (>3 Ki67-positive cells per acinus; *, $P < 0.05$; **, $P < 0.01$; data are means ± standard deviations). (D) Quantification of percentage of cleaved-caspase 3-positive acini.

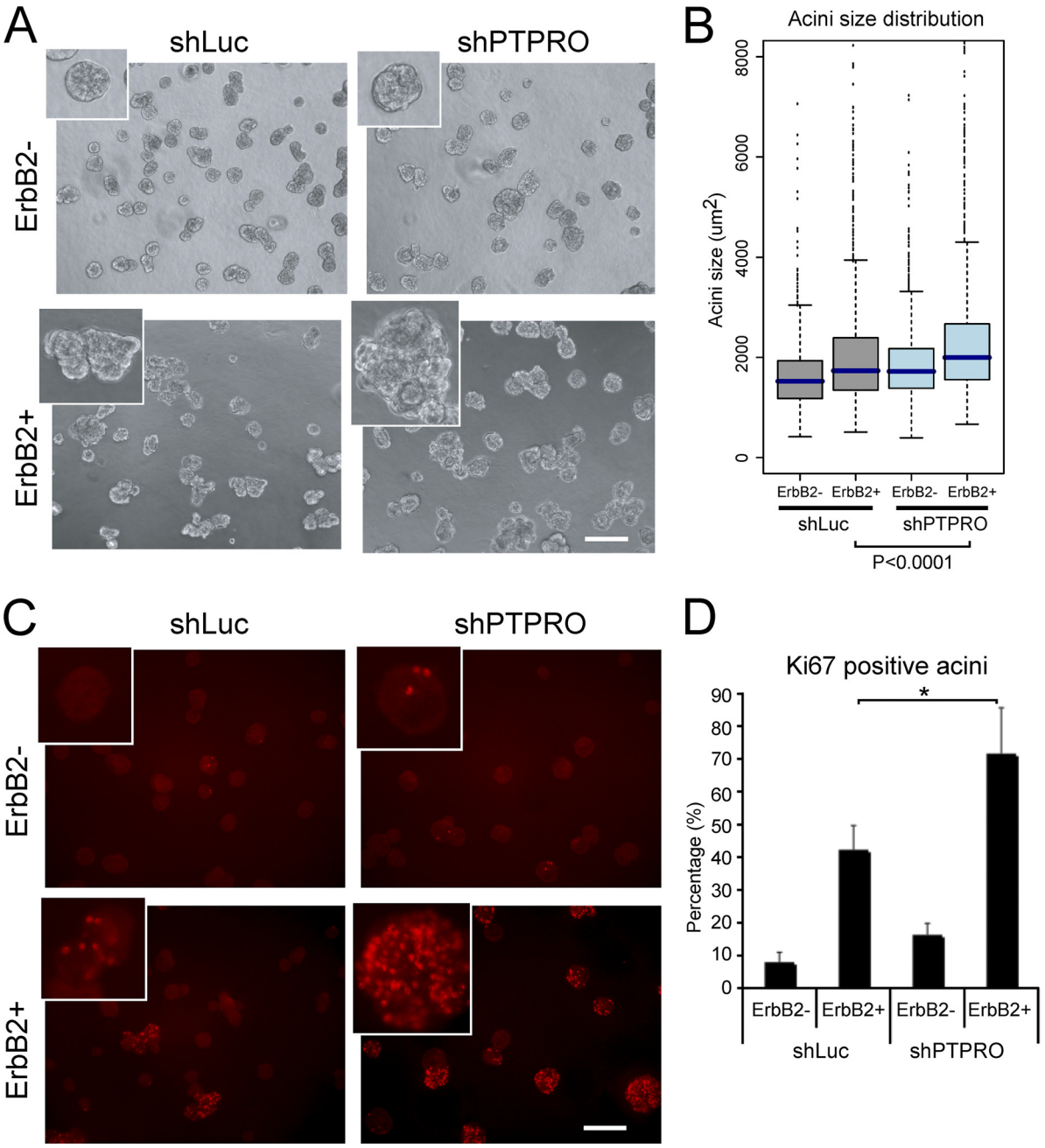

FIG 5 Suppression of PTPRO cooperated with ErbB2 to promote proliferation. (A) Phase images of day 12 acinar structures from 10A.B2.shPTPRO (shPTPRO) and control 10A.B2.shLuc (shLuc) cells with (bottom panels) or without (top panels) ErbB2 activation for 4 days. Scale bar = 100 μm. (B) Box plot for distribution of area of the acinar structures of these cell lines with (ErbB2+) or without (ErbB2−) ErbB2 activation. (C) Ki67 staining for day 18 acinar structures from shLuc or shPTPRO cells grown with (bottom panels) or without (top panels) ErbB2 activation for 2 days (red). Scale bar = 100 μm. (D) Plot of the percentage of Ki67-positive acini measured in these two cell lines for at least 600 acini from three independent experiments. *, $P < 0.05$.

ErbB2, we monitored changes in phosphotyrosine levels by immunofluorescence staining of 3D acini with antiphosphotyrosine antibodies. Our data revealed that tyrosine phosphorylation was upregulated following suppression of PTPRO, both in the absence and the presence of dimerizer (Fig. 6A).

To test whether PTPRO may directly dephosphorylate ErbB2, we immunoprecipitated the receptor from unstimulated PTPRO-suppressed cells and observed a 2.2-fold increase in tyrosine phosphorylation compared to ErbB2 from control cells (Fig. 6B), illustrating that ErbB2 phosphorylation was elevated upon loss of PTPRO. In addition to the increase in phosphorylation in unstimulated cells, activation of ErbB2 also resulted in a higher level of receptor phosphorylation (3.7-fold versus 5.0-fold) in PTPRO-suppressed cells (Fig. 6B). To determine if ErbB2 is a direct substrate of PTPRO, we used a strategy we had developed for investigating PTP-substrate relationships that involved production of a substrate-trapping mutant form of the phosphatases. By mutating to Ala the conserved acidic residue that functions as a gen-

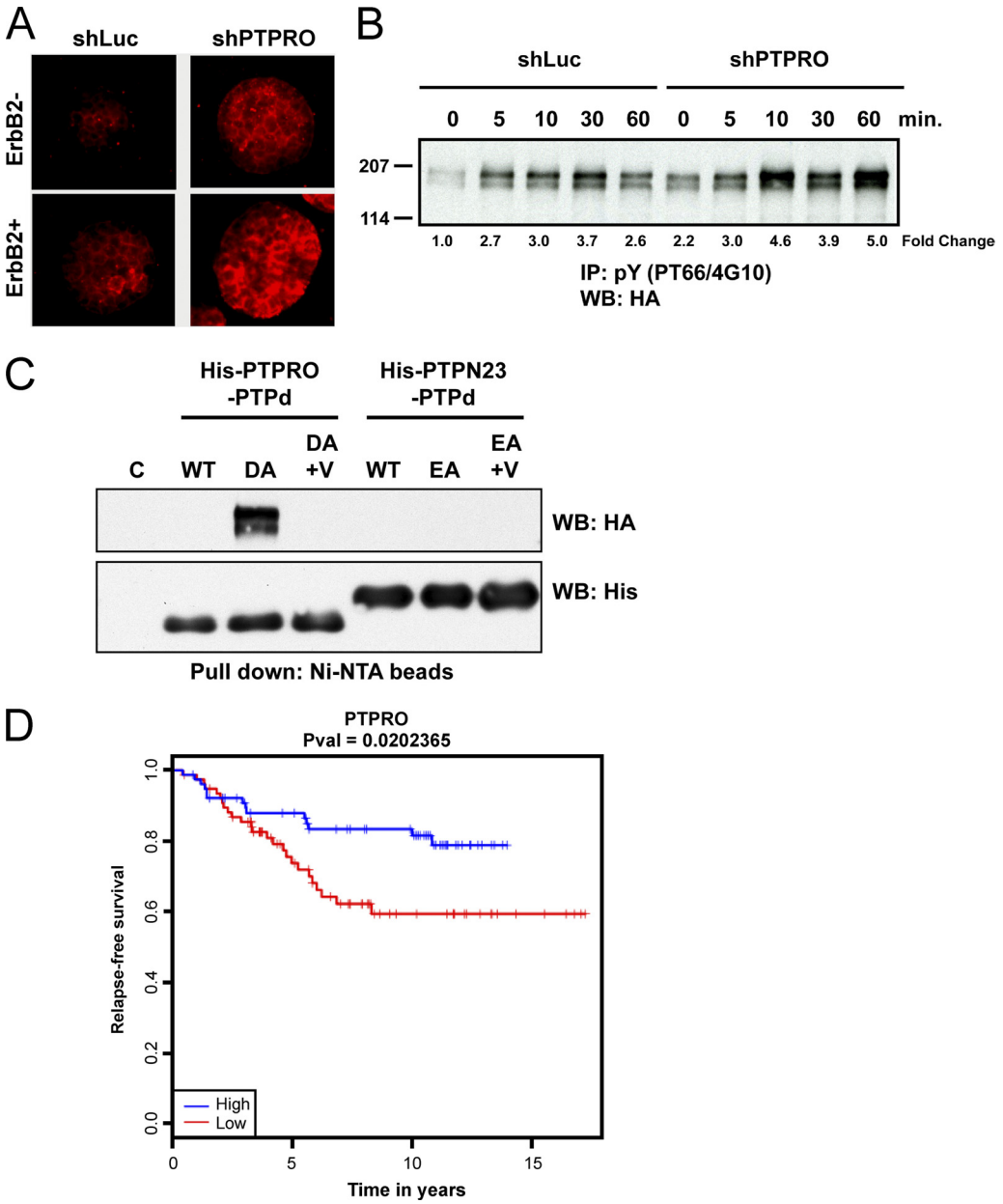

FIG 6 ErbB2 was a direct substrate of PTPRO. (A) Representative images of immunofluorescent staining of antiphosphotyrosine in 3D acini at day 18 with (bottom panels) or without (top panels) ErbB2 activation for 2 days. (B) Extracts from shLuc and shPTPRO cells with ErbB2 activation for different time points were first immunoprecipitated (IP) with antiphosphotyrosine (pY) antibody and then immunoblotted (WB) for ErbB2 with anti-HA antibody. (C) Purified recombinant His-tagged forms of the catalytic domain of PTPRO or PTPN23 were mixed with pervanadate-treated 10A.B2 cell lysates and then precipitated with Ni-NTA agarose beads. Binding of ErbB2 was assessed by blotting the precipitates with anti-HA antibodies. Anti-His tag antibody blot was used for loading control. C, empty bead control; WT, wild type; DA and EA, PTPRO-D1102A (DA) and PTPN23-E1357A (EA) substrate-trapping mutants in the absence or presence (+V) of vanadate. (D) Kaplan-Meier survival curve in ErbB2-overexpressing patients based on PTPRO expression levels. ErbB2-overexpressing patients were stratified into upper quartile ($n = 77$) and lower quartile ($n = 77$) based on the expression level of PTPRO.

eral acid in the first step of catalysis, we produced a form of the PTP that maintains a high affinity for its target substrates but in which catalytic turnover is severely impaired. Consequently, the substrate-trapping mutant can bind to its substrate, forming a stable complex that can be isolated by immunoprecipitation (11). In the 3D culture system, it is difficult to obtain a sufficient number of cells for biochemical analysis. Therefore, we treated MCF-10A cells expressing ErbB2 with pervanadate in 2D culture, to inactivate all the cellular PTPs and thereby to elevate the levels of tyrosine phosphorylation, and incubated the cell lysates with a substrate-trapping mutant form of PTPRO. We observed a direct, stable interaction between this mutant PTPRO and ErbB2, but not between the wild-type PTPRO and ErbB2 or between another phosphatase PTPN23 and ErbB2 (Fig. 6C), consistent with a direct enzyme-substrate interaction between the two.

Loss of PTPRO correlated with poor prognosis in ErbB2-overexpressing breast cancer patients. To investigate the clinical significance of changes in PTPRO expression for patients with ErbB2-positive cancers, we analyzed the relationship between the expression level of PTPRO and survival in ErbB2-overexpressing patients, using the curated data set described above. The expression levels of ErbB2 in 922 patients was ordered from high to low, and the top one-third of the ErbB2 high expressors ($n = 307$) were segregated for PTPRO expression into top ($n = 77$) and bottom ($n = 77$) quartiles. Kaplan-Meier survival analysis demonstrated a significant correlation between decreased PTPRO expression and shorter survival of ErbB2-overexpressing patients, compared to the survival observed for ErbB2-overexpressing patients expressing high levels of PTPRO ($P = 0.02$) (Fig. 6D). Thus, decrease in PTPRO expression is a clear poor-prognosis indicator for ErbB2-positive breast cancers.

DISCUSSION

We report identification of PTPRO as a novel regulator of mammary epithelial morphogenesis and a predictor of clinical prognosis for women with ErbB2-positive breast cancers.

PTPRO is an evolutionarily conserved receptor-type protein tyrosine phosphatase that was found to be hypermethylated in several cancers, including breast cancer (32), hepatomas (25), colon cancer (24), and lung cancer (25). The *PTPRO* gene is localized in the chromosomal region 12p12.3, which is characterized by loss of heterozygosity in different types of cancers (26). In this study, we have identified a novel role for PTPRO as a regulator of proliferation arrest during normal mammary epithelial morphogenesis and have demonstrated a direct correlation between downregulation of PTPRO expression and poor clinical prognosis in human breast cancer. Thus, our studies not only identify PTPRO as a regulator of mammary epithelial cell morphogenesis but also illustrate a novel context in which to understand how PTPRO functions as a tumor suppressor.

Our studies also demonstrated that gene expression patterns differ between mammary epithelial cells grown in 2D or 3D culture. There is an increasing body of evidence to suggest that mammary epithelial cells in 3D have distinct signaling properties (22, 28) compared to cells grown on 2D monolayer cultures, demonstrating that culture conditions can significantly affect activation of signaling pathways. It was not clear how cells in 2D and 3D use different pathways to reach proliferation arrest; nevertheless, these analyses highlight the need for further analysis for understanding how cells differ in 3D compared to 2D growth conditions. Furthermore, as shown in this study, 3D culture platforms enabled identification of PTPRO as a novel regulator of signaling in breast cancer that would have been missed otherwise, thus highlighting the need to include 3D cell culture platforms for discovery and validation of cancer-relevant targets.

ErbB2 (HER2 or Neu), which is a member of the ErbB family of receptor tyrosine kinases, is amplified or overexpressed in ~25% of breast cancer patients, where it correlates with poor prognosis and high invasiveness (36). In order to develop effective ways to treat patients with ErbB2-positive cancers, it is very important to develop a deeper understanding of the mechanisms by which the ErbB2 signaling pathway is regulated. Although the protein tyrosine phosphatases (PTPs) that function in a coordinated manner with ErbB2 will also be critical regulators of oncogenic signaling, their identity and function have not been characterized extensively. The PTPs may exert their effects at multiple levels. PTPN13 (PTP-BAS) (45) and PTPN9 (MEG2) (43) have been shown to dephosphorylate the C-terminal phosphotyrosine of ErbB2 directly and thereby inhibit ErbB2 signaling in breast cancer cell lines. ErbB2 itself has been shown to induce expression of several PTPs (44). Recently, we used an RNAi-mediated loss-of-function screen to identify three PTPs, PTPN23, PTPRG, and PTPRR, which inhibited mammary ErbB2-induced epithelial cell motility, and of which PTPN23 also inhibited ErbB2-induced mammary epithelial cell invasion (20). PTPN23 was shown to exert its effects by recognizing E-cadherin and β-catenin directly as the substrates, as well as dephosphorylating the autophosphorylation site in SRC, thereby inactivating the kinase. It is important to note that PTPs may also function positively, to promote oncogenic signaling. A receptor PTP, PTPε, has been shown to play an important role in ErbB2/NEU-mediated transformation, exerting its effects by dephosphorylating the inhibitory C-terminal site in SRC, thereby activating the kinase and functioning in a manner opposite to that of PTPN23 (12). In addition, PTP1B, which has been reported to be overexpressed in breast cancer coincident with overexpression of ErbB2 (40), plays a positive role in the development and metastasis of ErbB2-positive breast tumors, promoting ErbB2-induced signaling by a mechanism that includes dephosphorylation of p62DOK and activation of mitogen-activated protein (MAP) kinase (1, 17). Nevertheless, the roles of other PTPs in mammary epithelial cell tumors remain unclear. In this study, we have identified PTPRO as a novel regulator of ErbB2 signaling. Suppression of PTPRO in MCF-10A cells enhanced cellular proliferation and delayed proliferation arrest in 3D acini. Intriguingly, we find that PTPRO directly dephosphorylates ErbB2 and that suppression of PTPRO enhanced tyrosine phosphorylation of ErbB2 and promoted ErbB2-induced cell proliferation and transformation. Neither ErbB2-induced Erk1/2 nor Akt activation was altered in cells lacking PTPRO (see Fig. S6 in the supplemental material), suggesting that increased activation of ERK and Akt are not the mechanisms by which loss of PTPRO cooperates with ErbB2.

Our results identify PTPRO levels as an indicator of clinical outcome for ErbB2-positive patients, where lower levels of PTPRO significantly decreased relapse-free survival of patients with ErbB2-expressing breast cancers. These observations have major implications for breast cancer patients because amplification and overexpression of ErbB2 is strongly associated with poor clinical prognosis in node-positive patients. Although there are two targeted therapies (trastuzumab and lapatinib) that are used to treat patients with ErbB2-positive breast cancers, more than 50% of patients encounter either *de novo* or acquired resistance to trastuzumab (15, 29). Furthermore, 2 to 3% of patients who receive trastuzumab have a risk of congestive heart failure (34). Thus, there is a significant need to identify factors that are associated with good prognosis and to personalize the choice of treatment strategies. In addition, identification of novel regulators of ErbB2 signaling will facilitate the design of better ways to target the ErbB2 pathway in breast cancer patients.

ACKNOWLEDGMENTS

We thank members of the Muthuswamy and Tonks laboratory for insightful discussions.

This work was supported by grants CA098830 and BC075024, an Era of Hope Scholar award from the DOD Breast Cancer Research Program,

the Rita Allen Foundation, the Lee K. and Margaret Lau Chair for Breast Cancer Research, and the Campbell Family Institute for Breast Cancer Research to S.K.M. and by NIH grant CA53840 to N.K.T. Support was received from the Ontario Institute for Cancer Research through funding provided by the Government of Ontario to P.C.B. This work was also funded in part by the Ontario Ministry of Health and Long Term Care (OMOHLTC).

The views expressed in this article do not necessarily reflect those of the OMOHLTC.

REFERENCES

1. **Bentires-Alj M, Neel BG.** 2007. Protein-tyrosine phosphatase 1B (PTP1B) is required for HER2/Neu-induced breast cancer. Cancer Res. **67**:2420–2424.
2. **Bild AH, et al.** 2006. Oncogenic pathway signatures in human cancers as a guide to targeted therapies. Nature **439**:353–357.
3. **Chen B, Bixby JL.** 2005. A novel substrate of receptor tyrosine phosphatase PTPRO is required for nerve growth factor-induced process outgrowth. J. Neurosci. **25**:880–888.
4. **Chen L, Juszczynski P, Takeyama K, Aguiar RC, Shipp MA.** 2006. Protein tyrosine phosphatase receptor-type O truncated (PTPROt) regulates SYK phosphorylation, proximal B-cell-receptor signaling, and cellular proliferation. Blood **108**:3428–3433.
5. **Christov K, et al.** 1991. Proliferation of normal breast epithelial cells as shown by in vivo labeling with bromodeoxyuridine. Am. J. Pathol. **138**: 1371–1377.
6. **Clendening JW, et al.** 2010. Dysregulation of the mevalonate pathway promotes transformation. Proc. Natl. Acad. Sci. U. S. A. **107**:15051–15056.
7. **Debnath J, Brugge JS.** 2005. Modelling glandular epithelial cancers in three-dimensional cultures. Nat. Rev. Cancer **5**:675–688.
8. **Debnath J, et al.** 2002. The role of apoptosis in creating and maintaining luminal space within normal and oncogene-expressing mammary acini. Cell **111**:29–40.
9. **Debnath J, Muthuswamy SK, Brugge JS.** 2003. Morphogenesis and oncogenesis of MCF-10A mammary epithelial acini grown in three-dimensional basement membrane cultures. Methods **30**:256–268.
10. **Desmedt C, et al.** 2007. Strong time dependence of the 76-gene prognostic signature for node-negative breast cancer patients in the TRANSBIG multicenter independent validation series. Clin. Cancer Res. **13**:3207–3214.
11. **Flint AJ, Tiganis T, Barford D, Tonks NK.** 1997. Development of "substrate-trapping" mutants to identify physiological substrates of protein tyrosine phosphatases. Proc. Natl. Acad. Sci. U. S. A. **94**:1680–1685.
12. **Gil-Henn H, Elson A.** 2003. Tyrosine phosphatase-epsilon activates Src and supports the transformed phenotype of Neu-induced mammary tumor cells. J. Biol. Chem. **278**:15579–15586.
13. **Gonzalez-Brito MR, Bixby JL.** 2009. Protein tyrosine phosphatase receptor type O regulates development and function of the sensory nervous system. Mol. Cell. Neurosci. **42**:458–465.
14. **Granot-Attas S, Elson A.** 2008. Protein tyrosine phosphatases in osteoclast differentiation, adhesion, and bone resorption. Eur. J. Cell Biol. **87**:479–490.
15. **Hudis CA.** 2007. Trastuzumab—mechanism of action and use in clinical practice. N. Engl. J. Med. **357**:39–51.
16. **Irizarry RA, et al.** 2003. Exploration, normalization, and summaries of high density oligonucleotide array probe level data. Biostatistics **4**:249–264.
17. **Julien SG, et al.** 2007. Protein tyrosine phosphatase 1B deficiency or inhibition delays ErbB2-induced mammary tumorigenesis and protects from lung metastasis. Nat. Genet. **39**:338–346.
18. **Juszczynski P, et al.** 2009. BCL6 modulates tonic BCR signaling in diffuse large B-cell lymphomas by repressing the SYK phosphatase, PTPROt. Blood **114**:5315–5321.
19. **Kim M, Kim H, Jho EH.** 2010. Identification of ptpro as a novel target gene of Wnt signaling and its potential role as a receptor for Wnt. FEBS Lett. **584**:3923–3928.
20. **Lin G, Aranda V, Muthuswamy SK, Tonks NK.** 2011. Identification of PTPN23 as a novel regulator of cell invasion in mammary epithelial cells from a loss-of-function screen of the 'PTP-ome'. Genes Dev. **25**:1412–1425.
21. **Loi S, et al.** 2008. Predicting prognosis using molecular profiling in estrogen receptor-positive breast cancer treated with tamoxifen. BMC Genomics **9**:239. doi:10.1186/1471-2164-9-239.
22. **Martin KJ, Patrick DR, Bissell MJ, Fournier MV.** 2008. Prognostic breast cancer signature identified from 3D culture model accurately predicts clinical outcome across independent datasets. PLoS One **3**(8):e2994. doi: 10.1371/journal.pone.0002994.
23. **Miller LD, et al.** 2005. An expression signature for p53 status in human breast cancer predicts mutation status, transcriptional effects, and patient survival. Proc. Natl. Acad. Sci. U. S. A. **102**:13550–13555.
24. **Mori Y, et al.** 2004. Identification of genes uniquely involved in frequent microsatellite instability colon carcinogenesis by expression profiling combined with epigenetic scanning. Cancer Res. **64**:2434–2438.
25. **Motiwala T, et al.** 2003. Suppression of the protein tyrosine phosphatase receptor type O gene (PTPRO) by methylation in hepatocellular carcinomas. Oncogene **22**:6319–6331.
26. **Motiwala T, et al.** 2004. Protein tyrosine phosphatase receptor-type O (PTPRO) exhibits characteristics of a candidate tumor suppressor in human lung cancer. Proc. Natl. Acad. Sci. U. S. A. **101**:13844–13849.
27. **Motiwala T, et al.** 2009. PTPROt inactivates the oncogenic fusion protein BCR/ABL and suppresses transformation of K562 cells. J. Biol. Chem. **284**:455–464.
28. **Muthuswamy SK.** 2011. 3D culture reveals a signaling network. Breast Cancer Res. **13**:103.
29. **Muthuswamy, SK.** 2011. Trastuzumab resistance: all roads lead to SRC. Nat. Med. **17**:416–418.
30. **Muthuswamy SK, Li D, Lelievre S, Bissell MJ, Brugge JS.** 2001. ErbB2, but not ErbB1, reinitiates proliferation and induces luminal repopulation in epithelial acini. Nat. Cell Biol. **3**:785–792.
31. **Pawitan Y, et al.** 2005. Gene expression profiling spares early breast cancer patients from adjuvant therapy: derived and validated in two population-based cohorts. Breast Cancer Res. **7**:R953–R964.
32. **Ramaswamy B, et al.** 2009. Estrogen-mediated suppression of the gene encoding protein tyrosine phosphatase PTPRO in human breast cancer: mechanism and role in tamoxifen sensitivity. Mol. Endocrinol. **23**:176–187.
33. **Saeed AI, et al.** 2003. TM4: a free, open-source system for microarray data management and analysis. Biotechniques **34**:374–378.
34. **Seidman A, et al.** 2002. Cardiac dysfunction in the trastuzumab clinical trials experience. J. Clin. Oncol. **20**:1215–1221.
35. **Shintani T, et al.** 2006. Eph receptors are negatively controlled by protein tyrosine phosphatase receptor type O. Nat. Neurosci. **9**:761–769.
36. **Slamon DJ, et al.** 1987. Human breast cancer: correlation of relapse and survival with amplification of Her-2/*neu* oncogene. Science **235**:177–182.
37. **Sotiriou C, et al.** 2006. Gene expression profiling in breast cancer: understanding the molecular basis of histologic grade to improve prognosis. J. Natl. Cancer Inst. **98**:262–272.
38. **Taniguchi Y, London R, Schinkmann K, Jiang S, Avraham H.** 1999. The receptor protein tyrosine phosphatase, PTP-RO, is upregulated during megakaryocyte differentiation and is associated with the c-Kit receptor. Blood **94**:539–549.
39. **Thomas PE, et al.** 1994. GLEPP1, a renal glomerular epithelial cell (podocyte) membrane protein-tyrosine phosphatase. Identification, molecular cloning, and characterization in rabbit. J. Biol. Chem. **269**:19953–19962.
40. **Wiener JR, et al.** 1994. Overexpression of the protein tyrosine phosphatase PTP1B in human breast cancer: association with p185c-erbB-2 protein expression. J. Natl. Cancer Inst. **86**:372–378.
41. **Wiggins RC, Wiggins JE, Goyal M, Wharram BL, Thomas PE.** 1995. Molecular cloning of cDNAs encoding human GLEPP1, a membrane protein tyrosine phosphatase: characterization of the GLEPP1 protein distribution in human kidney and assignment of the GLEPP1 gene to human chromosome 12p12-p13. Genomics **27**:174–181.
42. **Wu G, Feng X, Stein L.** 2010. A human functional protein interaction network and its application to cancer data analysis. Genome Biol. **11**(5): R53. doi:10.1186/gb-2010-11-5-r53.
43. **Yuan T, Wang Y, Zhao ZJ, Gu H.** 2010. Protein-tyrosine phosphatase PTPN9 negatively regulates ErbB2 and epidermal growth factor receptor signaling in breast cancer cells. J. Biol. Chem. **285**:14861–14870.
44. **Zhai YF, et al.** 1993. Increased expression of specific protein tyrosine phosphatases in human breast epithelial cells neoplastically transformed by the neu oncogene. Cancer Res. **53**(10 Suppl):2272–2278.
45. **Zhu J-H, et al.** 2008. Protein tyrosine phosphatase PTPN13 negatively regulates Her2/ErbB2 malignant signaling. Oncogene **27**:2525–2531.